International Journal of Scientific and Technical Research in Engineering (IJSTRE)
www.ijstre.com Volume 4 Issue 6 ǁ Nov-Dec 2019.
ISSN: 2581-9941

Generation of Mathematical Models to Predict the Chip Morphology for Ti-6Al-4V Alloy during Turning Operation

Michael Kwabena Boadu[1], Ebenezer Omari Abankwa[2], Listowel Abugri Anaba[3]
[1,2]*Department of Mechanical and Industrial Engineering, University for Development Studies, Ghana*
[3]*Department of Agricultural Engineering, University for Development Studies, Ghana*

Abstract: *Chip morphology is highly necessary to examine the machinability of titanium alloys during turning operations. The main goal of this research work was to generate mathematical models for chip morphology parameters such as peak height, valley height, tooth pitch, localised shear angle and bulge angle using MINITAB 17 Statistical Software. The models were proven to be valid since their average percentage errors fell within* $\pm$ 5.0. *The optimal cutting conditions for the chip morphology parameters were also determined.*
Keywords: *Alloy, Chip, Mathematical Models, Morphology, Ti-6Al-4V, Turning Operation.*

I.Introduction

Chip morphology is relevant for studying the machinability of titanium alloys and gaining genuine understanding of the fundamental phenomena governing machinability, such as mechanics of machining process, thermal aspects associated with the cutting process, vibrations and others [1]. It is of no doubt that machining of titanium alloys (Ti-alloys) is quite challenging since these super alloys even maintain their high strength at the higher temperatures produced during machining. Some other factors which make it difficult to machine Ti-alloys are caused by low thermal conductivity, high coefficient of friction between the chip and the cutting tool interface, high work-hardening tendency, and a strong capacity to chemical reactivity at the cutting temperatures (> 500°C) with almost all tool materials [2]. According to Ezugwu [3], these peculiar properties have made the machining of Ti-alloys highly difficult. For these and other significant problems, Ti-alloys are classified as difficult-to-machine materials. However, Nabhani [4] and Ribeiro et al. [5] showcased that Ti-6Al-4V is one of the most widely used Ti-alloys due to the fact that it is more versatile than other Ti-alloys.

In Ti-6Al-4V alloy, segmented chips are formed at low cutting speeds comparative to other materials in which chip segmentation occurs at relatively high cutting speeds [6]. Shaw et al. [7] investigated the influence of cutting speed and feed rate on tooth pitch, specific cutting energy and cutting ratio for Ti-6Al-4V alloy. They found tooth pitch independent of cutting speed but observed a linear increase with increase in feed rate. Specific cutting energy was found to decrease with increase in cutting speed and feed rate. However, decrease in case of feed rate was exponential. Cutting ratio was reported as independent of cutting speed whereas it increased with increase in feed rate [8]. Hua and Shivpuri [9] developed a FEM model based on crack initiation for prediction of chip morphology and segmentation in orthogonal machining of Ti-6Al-4V alloy. Based on a simulation study they concluded that with increase in cutting speed, crack propagation shifts from tool tip to the free surface of the deformed chip in shear zone, changing the chip from discontinuous to a serrated one.

Gente et al. [10] studied chip formation in Ti-6Al-4V alloy in the cutting speed range of 300 m/min to 6000 m/min. They utilized a quick stop technique that was able to generate rapid deceleration from 2500 m/min in a very short distance. When cutting speed and chip thickness was increased beyond 2000 m/min and 50 μm respectively, partially separated segments were observed. Also, the shear strain was found almost independent of cutting parameters. Sun et al. [11] observed that the force frequency of cyclic force produced during the formation of segmented chips was the same as the chip segmentation frequency. Bayoumi and Xie [12] investigated the metallurgical aspects of shear localized chip formation in Ti-6Al-4V alloy. Study of the influence of cutting parameters on shear band formation and shear banding frequency was also carried out. They stated that a segmented chip which contains some evidence for shear localization is easier to break and relatively ideal to dispose for automated machining.

Wan et al. [13] studied the variation of segment spacing, adiabatic shear bandwidth and degree of segmentation with cutting speed, feed rate and rake angle. They found an increase in the value of the above mentioned parameters with increase in cutting speed and feed rate, and decrease in rake angle. Sun and Guo [14] characterized the morphology of top surface, free surface, back surface and cross section surface of chips obtained in end milling. The microstructural analysis showed that β phase experiences severe deformation and transformation to α phase in the second shear zone and thus, the phase transformation subsequently leads to microhardness variations characterized by higher hardness at the surface and the lower hardness in the immediate subsurface. They also observed that the shear band as well as the corner section of the chip shows increased hardness. Boadu et al. [15] generated predictive models for chip morphology parameters (such as chip length,

chip width, chip thickness and shear band) of aluminum metal matrix composites in end milling machining utilizing MINITAB 17 Statistical Software. The models were proven to be valid except for that of chip thickness whose average percentage error fell outside 5.0. The optimal cutting conditions for the chip morphology parameters were also determined. Kouadri et al. [16] in their study proposed chip segmentation frequency and chip segmentation length to quantify segmented chip morphology. Komanduri et al. [17] studied the chip formation process during the cutting of Ti–6Al–4V and proposed the well-known 'catastrophic shear chip' theory. They concluded that the 'catastrophic shear chip' exists in all speed ranges and is independent of tool geometry. However, this theory cannot be utilized to explain why the chip morphology is different under different cutting speeds.

Analyzing different titanium chips at cutting speed ranges of 1 in./min to 300 ft./min, Cook [18] attributed the difference in morphology between the chips at high speed and low speed to the temperature produced during the cutting process. According to the author, the higher the cutting speed, the greater the temperature in the primary deformation zone. When the temperature softening influence in the primary deformation zone is greater than the strain hardening effect, the chip becomes serrated. It is clear from the previous studies that cutting speed has an influence on chip morphology but less work has been done to predict the chip morphology inclusive of the other cutting parameters such as depth of cut and feed during end milling machining. Yameogo et al. [19] developed a model to predict the chip formation under orthogonal cutting configuration utilizing a 2D finite element approach with Abaqus/Explicit code which is based on the Lagrangian formulation. Liu and Shi [20] generated a finite element model to predict the chip formation and phase transformation in orthogonal machining of hardened AISI 52100 steel (62HRC) using Polycristalline Cubic Boron Nitride (PCBN) tools. The model basically takes into account chip separation criterion based on critical equivalent plastic strain; a Coulomb's law for the friction at the tool/chip interface; a material constitutive relation of velocity-modified temperature; a thermal analysis involving the heat released from inelastic deformation energy and friction; and an annealing effect model, in which the work hardening effect may be lost or re-accumulate depending on material temperature. This research work seeks to generate predictive models for chip morphology parameters such as Peak height (t_p), valley height (t_v), tooth pitch (p_c), localized shear angle ($\emptyset seg$) and bulge angle (ρ_{seg}). It also seeks to validate the models and to generate optimal morphology parameters which would improve the tool life.

II.Material

Titanium Ti6Al4V is the prime alloy of the titanium industry, also known as Grade 5, TA6V or Ti64. This α-β titanium-based alloy is the most commonly used of all titanium alloys and accounts for 50% of total titanium usage in the world. Phase stabilizers are Aluminium and Vanadium. Al reduces density, stabilizes and strengthens α while vanadium provides a greater amount of the more ductile β phase for hot-working [21]. Titanium Ti6Al4V has an elastic modulus of 113.8 GPa and a tensile strength of 993 MPa. It also has an elongation of 14% and yield strength of 924 MPa [22]. Titanium Ti6Al4V has a poisson's ratio of 0.34, density of 4.43 x 1000 kgm^{-3}, hardness of 36 HRC, an impact strength of 19 J and thermal expansion of 8.6 10^{-6}/ ℃ [22]. The chemical composition of Ti-6Al-4V alloy is presented below in Table 1. The choice of the material was based on the paper published by Upadhyay et al. [1].

Table 1: Chemical composition of Ti-6Al-4V alloy

Element	C	Fe	N_2	O_2	Al	V	Ti
Content %	< 0.08 %	< 0.25 %	< 0.05 %	< 0.2 %	5.50-6.76 %	3.5-4.5 %	Balance

Source: Azom.com [23]

III.Method

The data used in this research work was obtained from the paper published by Upadhyay et al. [1]. MINITAB 17 Statistical Software was used to generate predictive models, residual plots and optimal values for the chip morphology parameters. The data in Table 2 depicts the effects of cutting conditions on peak height, valley height, tooth pitch, localised shear angle and bulge angle.

Table 2: Effects of cutting conditions on chip morphology parameters

V *(mm/min)*	f *(mm/rev)*	d *(mm)*	t_p (μm)	t_v (μm)	p_c (μm)	$\emptyset_{seg}$ *(degree)*	ρ_{seg} *(degree)*
50	0.16	1.5	206	125	106	32.40	26.19
90	0.16	1.5	199	112	108	39.60	22.10
50	0.24	1.5	284	162	144	35.96	21.59
90	0.24	1.5	266	145	147	38.60	20.47
50	0.20	1	256	156	111	33.98	22.82
90	0.20	1	241	138	125	38.20	20.37
50	0.20	2	257	153	114	32.39	24.19
90	0.20	2	242	138	124	33.85	23.90
70	0.16	1	208	121	102	32.57	26.52
70	0.24	1	281	160	143	36.36	24.56
70	0.16	2	211	123	105	34.38	27.04
70	0.24	2	287	164	154	36.83	20.63
70	0.20	1.5	242	142	121	33.61	24.35
70	0.20	1.5	249	144	118	34.29	24.48
70	0.20	1.5	250	147	120	33.04	25.83

Courtesy: Upadhyay et al. [1]

3.1 Generation and Validation of Models

Minitab 17.0 Statistical Software was used to generate the various models for chip morphology. The models are in second order. In the process, the R^2 values for each chip morphology parameter was also generated. Each model shows three different two-way interactions. In the case of validation, Minitab 17.0 was also used to generate the predicted values.

3.1.1 Modeling of Chip Morphology Parameters

The uncoded models generated by Minitab 17.0 for the chip morphology parameters are in second order and respectively written as shown in Equation (1) - (5)

t_p = 44.6 + 0.344 V + 1103 f - 4.8 d - 3.44 V * f + 0.000 V * d + 38 f * d (1)

t_v = 72.6 - 0.256 V + 519 f - 9.5 d - 1.25 V * f + 0.075 V * d + 25 f * d (2)

p_c = 23.6 + 0.269 V + 350 f - 9.0 d + 0.31 V * f - 0.100 V * d + 100 f * d (3)

$\emptyset_{seg}$ = -8.1 + 0.486 V + 152 f + 7.3 d - 1.42 V * f - 0.0690 V * d - 16.8 f * d (4)

ρ_{seg} = 37.7 - 0.316 V - 27 f + 7.7 d + 0.93 V * f + 0.0540 V * d - 55.6 f * d (5)

Where t_p= Peak height; t_v = valley height; p_c= tooth pitch; $\emptyset_{seg}$= localized shear angle; ρ_{seg}= bulge angle; V = cutting speed; f = feed rate and d = depth of cut. The R^2 values for peak height, valley height, tooth pitch, localized shear angle and bulge angle were respectively 97.46 %, 92.50 %, 92.84 %, 62.12 % and 61.10 %. This implies that the models for peak height, valley height and tooth pitch fit the data well. The R^2 values for localized shear angle (62.12 %) and bulge angle (61.10 %) designate that the corresponding models for these parameters moderately fit the data.

3.1.2 Validation of Models

To ascertain the validity of the models, the experimental values for the response variables were compared to that of their corresponding predicted values. The standard percentage error considered for this research work was $\pm$ 5.0. When the average percentage error falls within $\pm$ 5.0 range then it means the model is valid and can be utilized for subsequent prediction of the response variable. The percentage error was calculated using Equation (6):

$$\text{Percentage Error} = \frac{Experimental\ value - Predicted\ value}{Experimental\ value} \times 100\% \quad (6)$$

Tables 3,4,5,6 and 7 present the comparison of experimental and predicted values of peak height, valley height, tooth pitch, localized shear angle and bulge angle respectively.

Table 3: Comparison of Experimental Values with Predicted Values of Peak height

Experimental value	Predicted value	% Error
206	212.64	-3.22
199	204.39	-2.71
284	291.64	-2.69
266	272.39	-2.40
256	250.77	2.04
241	237.02	1.65
257	253.52	1.35
242	239.77	0.92
208	207.89	0.05
281	279.89	0.40
211	209.14	0.88
287	284.14	1.00
242	245.27	-1.35
249	245.27	1.50
250	245.27	1.89

Table 4 Comparison of Experimental Values with Predicted Values of Valley Height

Experimental value	Predicted value	% Error
125	130.13	-4.10
112	116.38	-3.91
162	169.63	-4.71
145	151.88	-4.74
156	150.25	3.69
138	133.00	3.62
153	149.50	2.29
138	135.25	1.99
121	123.38	-1.97
160	159.88	0.08
123	123.13	-0.11
164	161.63	1.45
142	142.00	0.00
144	142.00	1.39
147	142.00	3.40

Table 5 Comparison of Experimental Values with Predicted Values of Tooth Pitch

Experimental value	Predicted value	% Error
106	98.55	7.03
108	105.30	2.50
144	139.80	2.92
147	147.55	-0.37
111	116.18	-4.67
125	125.43	-0.34
114	122.18	-7.18
124	127.43	-2.77
102	101.93	0.07
143	139.68	2.32
105	101.93	2.92
154	147.68	4.10
121	122.80	-1.49
118	122.80	-4.07
120	122.80	-2.33

Table 6 Comparison of Experimental Values with Predicted Values of Localised Shear Angle

Experimental value	Predicted value	% Error
32.40	30.89	4.66
39.60	37.05	6.44
35.96	35.37	1.64
38.60	36.97	4.22
33.98	32.90	3.18
38.20	38.16	0.10
32.39	33.36	-2.99
33.85	35.86	-5.94
32.57	34.09	-4.67
36.36	36.96	-1.65
34.38	33.85	1.54
36.83	35.38	3.94
33.61	35.07	-4.34
34.29	35.07	-2.27
33.04	35.07	-6.14

Table 7 Comparison of Experimental Values with Predicted Values of Bulge Angle

Experimental value	Predicted value	% Error
26.19	27.23	-3.97
22.10	23.76	-7.51
21.59	22.10	-2.36
20.47	21.59	-5.47
22.82	25.02	-9.64
20.37	21.95	-7.76
24.19	24.31	-0.50
23.90	23.40	2.09
26.52	24.20	8.75
24.56	22.77	7.29
27.04	26.79	0.92
20.63	20.92	-1.41
24.35	23.67	2.79
24.48	23.67	3.31
25.83	23.67	8.36

From Table 3, the average percentage error for predicting peak height is -0.05 which falls within the range of $\pm$5.0 and thus, renders its corresponding model valid for subsequent predictions of peak height. From Table 4, the average percentage error for valley height prediction was found to be -0.11. This value (-0.11) falls within $\pm$5.0 and thus, the model for valley height is said to be valid and can be used for the prediction of valley height. Also, from Table 5, the average percentage error for tooth pitch (-0.09) falls within the range of the standard percentage error ($\pm$5.0). This shows that the mathematical model for tooth pitch is valid and can be used for subsequent predictions. Moreover, from Table 6, the mean percentage error for localised shear angle is -0.15. This value (-0.15) falls within the range of $\pm$5.0 and this implies that the mathematical model for localised shear angle is valid. Finally, from Table 7, the average percentage error for predicting bulge angle is -0.34. The percentage error in this case falls within the range of the standard percentage error ($\pm$5.0). It can however, be affirmed that the model for bulge angle is valid and can be used for subsequent predictions.

IV.Analysis Of Standardized Residuals For Chip Morphology Parameters

The difference between the observed and the fitted response value is known as residual. Each data point has one residual. Figures 1,2,3,4 and 5 show residual plots for peak height, valley height, tooth pitch, localized shear angle and bulge angle respectively. Included in the plots are normal probability plot, histograms, versus fits and versus order plots.

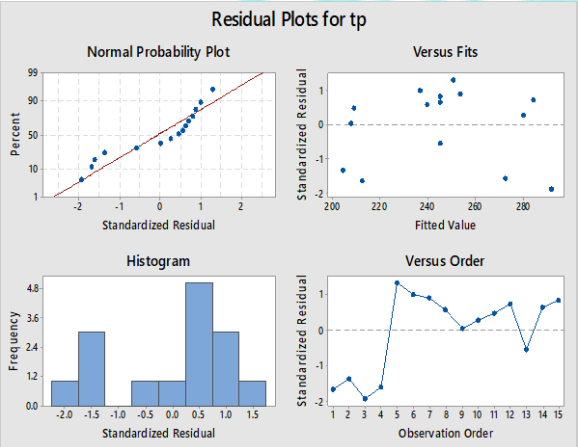

Figure 1: Residual Plot for Peak Height

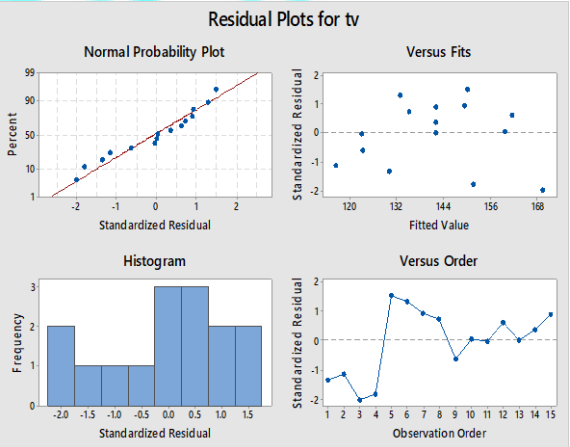

Figure 2: Residual Plots for Valley Height

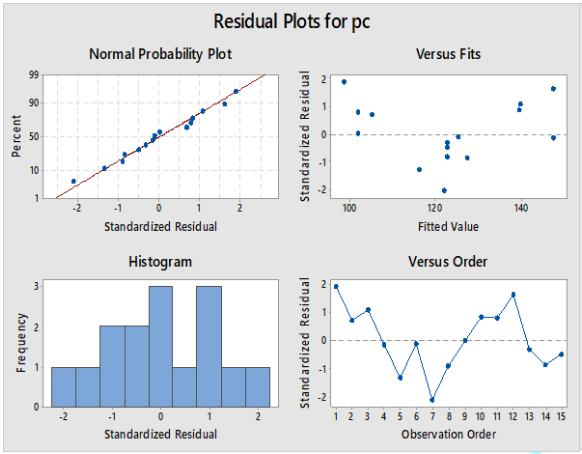

Figure 3: Residual Plot for Tooth Pitch

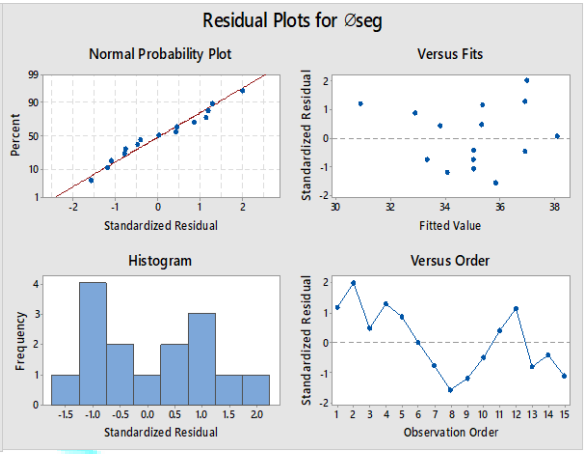

Figure 4: Residual Plots for Localised Shear Angle

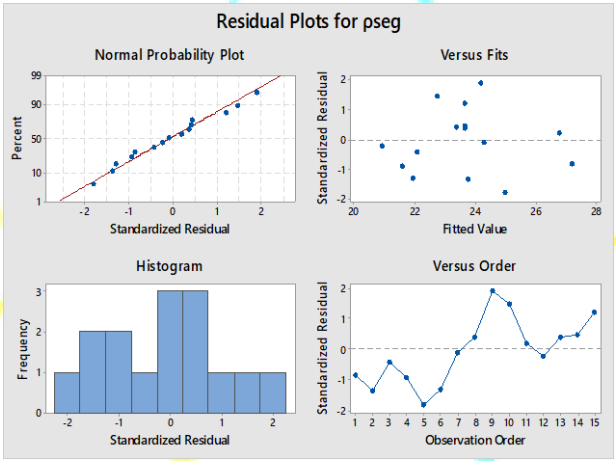

Figure 5: Residual Plots for Bulge Angle

The normal probability plot of the residuals is utilized to investigate the normality of the treatment data. If the distribution of residuals is normal, the plot will resemble a straight line. From the residual plots of all the chip morphology parameters (peak height, valley height, tooth pitch, localized shear angle and bulge angle) most of the plotted points lie closer to the distribution line and thus, affirming that the distribution of their residuals is normal.

Residuals versus order plot shows whether there are methodical effects in the data as a result of period or order of information gathering. From the residual plots of the morphology parameters, the residuals do not appear to follow a pattern on both sides of 0. This shows that their error terms are not correlated with one another.

The standardized residual versus fits plot shows whether the variance is constant, nonlinear relationship or outliers exist for the observations of each treatment data. The residual plots of Peak height, valley height, tooth pitch, localized shear angle and bulge angle do not show a common pattern of standardized residuals on both sides of 0. This shows that the variance of the error terms is constant for all the observations of each treatment data.

The histogram of standardized residuals shows the distribution of the standardized residuals for all observations. The histogram of the standardized residuals from the plots do not portray a bell-shape. However, its normality is tested from its corresponding normal probability plot which shows that the standardized residuals of peak height, valley height, tooth pitch, localized shear angle and bulge angle are normally distributed. The space between the bars shows the presence of an outlier for peak height.

V.Optimization Of Chip Morphology Parameters

Chip morphology parameters play a major role in improving the tool life. In this case, the chip morphology parameters such as peak height, valley height, localised shear angle and bulge angle must be minimized to enhance the tool life. The tooth pitch should be maximized in this regard. Figure 6 shows an optimization plot of peak height during the turning process.

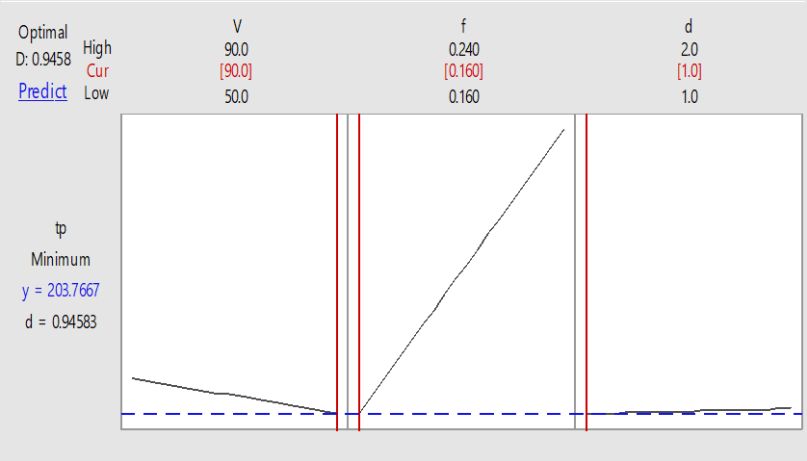

Figure 6: Optimization Plot for Peak Height

From the plot, the optimal cutting conditions for peak height is found to be at high cutting speed (90.0 rpm), low feed (0.160 mm/rev) and low depth of cut (1.0 mm). The optimal values are shown in red on the plot. The main goal is to minimize the peak height. Minimizing the peak height would enhance chip segmentation which increases chip breakage. This would eventually reduce cutting tool wear. All the machining parameters have a composite desirability of 0.95.

Figure 7 denotes an optimization plot of valley height during the turning process. From the plot, the optimal cutting conditions for valley height are found to be at high cutting speed (90.0 rpm), low feed (0.160 mm/rev) and low depth of cut (1.0 mm). The optimal values are shown in red on the plot. The main target is to minimize the valley height. Minimizing the peak height would enhance chip segmentation which increases chip breakage. This would eventually decrease cutting tool wear. All the cutting parameters have a composite desirability of 0.93.

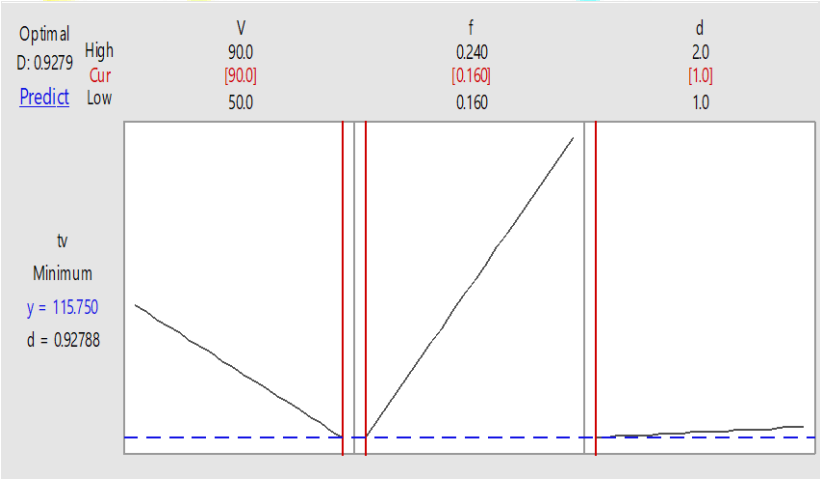

Figure 7: Optimization Plot for Valley Height

Figure 8 showcases an optimization plot of tooth pitch during the turning process. From the plot, the optimal cutting parameters for tooth pitch are found to be at high cutting speed (90.0 rpm), high feed (0.240 mm/rev) and high depth of cut (2.0 mm). The optimal values are shown in red on the plot. The main target is to maximize the tooth pitch. Maximizing the tooth pitch would enhance chip segmentation which increases chip breakage. This would eventually decrease cutting tool wear. All the cutting parameters have a composite desirability of 0.93.

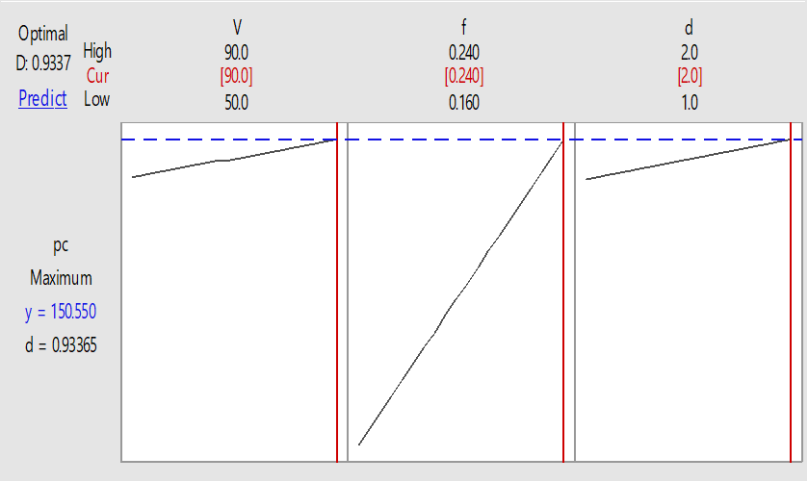

Figure 8: Optimization Plot for Tooth Pitch

Figure 9 denotes an optimization plot of localised shear angle during the turning process. From the plot, the optimal cutting parameters for localised shear angle is found to be at low cutting speed (50.0 rpm), low feed (0.160 mm/rev) and low depth of cut (1.0 mm). The optimal values are shown in red on the plot. The main target is to minimize the localised shear angle. Minimizing the localised shear angle increases the tooth height which enhances chip segmentation. Enhancing chip segmentation increases chip breakage which would eventually decrease the cutting tool wear. All the cutting conditions have a composite desirability of 1.00

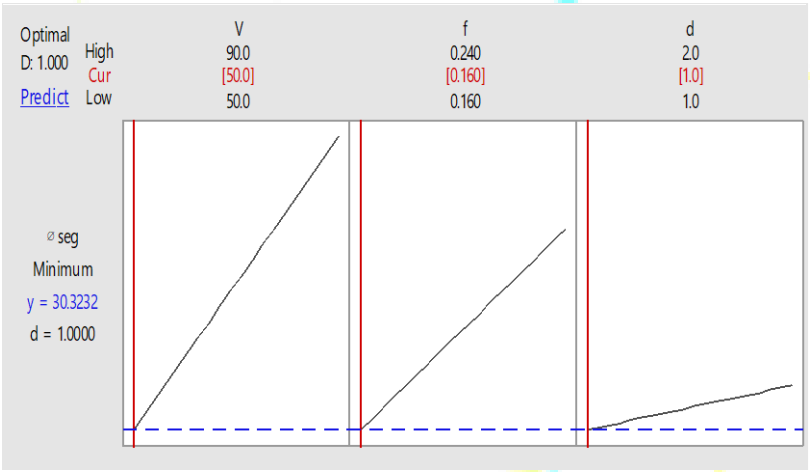

Figure 9: Optimization Plot for Localised Shear Angle

Figure 10 shows an optimization plot of bulge angle during the turning process. From the plot, the optimal cutting parameters for bulge angle is found to be at low cutting speed (50.0 rpm), high feed (0.240 mm/rev) and high depth of cut (2.0 mm). The optimal values are shown in red on the plot. The main goal is to minimize the bulge angle. Decreasing the bulge angle increases the tooth height which enhances chip segmentation. Enhancing chip segmentation increases chip breakage which would eventually improve the cutting tool life. All the cutting conditions have a composite desirability of 0.96.

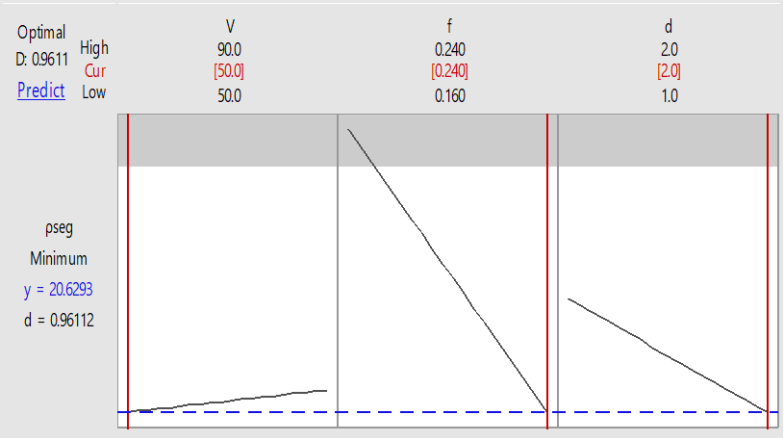

Figure 10: Optimization Plot for Bulge Angle

VI.Conclusions

This work has unarguably predicted the chip morphology for Ti-6Al-4V alloy during turning operation. The specific objectives were: 1. to generate predictive models for chip morphology parameters such as peak height, valley height, tooth pitch, localised shear angle and bulge angle using MINITAB 17 Statistical Software, 2. to validate the models and 3. to optimize the chip morphology parameters. The models generated satisfactorily predicted most of the morphology parameters. The R^2 value for peak height, valley height and tooth pitch was respectively 97.46 %, 92.50 % and 92.84 % and thus, showed that the models fit the data well. The R^2 value for localised shear angle and bulge angle was respectively 62.12 % and 61.10 % which showed that the models moderately fit the data. Predictive equations for peak height, valley height, tooth pitch, localised shear angle and bulge angle were found to be valid since their average percentage errors fell within ± 5.0. Moreover, the standardized residuals for peak height, valley height, tooth pitch, localised shear angle and bulge angle had a normal distribution. The variance for the error terms for all the chip morphology parameters were constant for all the observations of each treatment data. Also, the error terms for all the chip morphology parameters were not correlated with one another. Lastly, the optimal cutting conditions for peak height were found to be at high cutting speed (90.0 rpm), low feed (0.160 mm/rev) and low depth of cut (1.0 mm). For valley height, the optimal machining conditions were found to be at high cutting speed (90.0 rpm), low feed (0.160 mm/rev) and low depth of cut (1.0 mm). For tooth pitch, the optimal cutting conditions were found to be at high cutting speed (90.0 rpm), high feed (0.240 mm/rev) and high depth of cut (2.0 mm). For localised shear angle, the optimal cutting conditions were found to be at low cutting speed (50.0 rpm), high feed (0.240 mm/rev) and high depth of cut (2.0 mm). Also, the optimal cutting parameters for bulge angle was found to be at low cutting speed (50.0 rpm), high feed (0.240 mm/rev) and high depth of cut (2.0 mm).

REFERENCES

[1] Upadhyay, V., Jain, P.K. and Mehta, N.K. (2014). Comprehensive study of chip morphology in turning of Ti-6Al-4V, 5th International & 26th All India Manufacturing Technology, Design and Research Conference, IIT Guwahati, Assam, India.

[2] Ahsan, K. B., Mazid, A. M. and Pang, G.K.H. (2016). Morphological investigation of Ti-6Al-4V chips produced by conventional turning, Int. J. Machining and Machinability of Materials, Vol. 18, Nos. 1/2, pp. 138-154

[3] Ezugwu, E.O. (2005). Key improvements in the machining of difficult-to-cut aerospace super-alloys, International Journal of Machine Tools and Manufacture, Vol. 45, No. 12–13, pp. 1353–1367.

[4] Nabhani, F. (2001). Machining of aerospace titanium alloys, Robotics and Computer-Integrated Manufacturing, Vol. 17, No. 1, pp. 99–106.

[5] Ribeiro, M.V., Moreira, M.R.V. and Ferreira, J.R. (2003). Optimization of titanium alloy (6Al-4V) machining, Journal of Materials Processing Technology, Vols. 143–144, pp. 458–463.

[6] Calamaz, M., Coupard, D. and Girot, F. (2008). A new material model for 2D numerical simulation of serrated chip formation when machining titanium alloy Ti-6Al-4V, International Journal of Machine Tools and Manufacture, Vol. 48, No. 3, pp. 275–288.

[7] Shaw, M.C., Janakiram, M. and Vyas, A. (1991). The role of fracture in metal cutting chip formation, SME, NSF Grantees conference, Austin, Texas. pp. 359-366.

[8] Shaw, M.C. (2005). Metal cutting principles, Oxford Univ. Press, New York.

[9] Hua, J. and Shivpuri, R. (2004). Prediction of chip morphology and segmentation during the machining of Titanium alloys. Journal of Materials Processing Technology, Vol. 150, pp. 124-133.

[10] Gente, A., Hoffmeister, H.W. and Evans, C.J. (2001). Chip formation in machining Ti6Al4V at extremely high cutting speeds, CIRP Annals- Manufacturing Technology, Vol. 50, pp. 49-52.

[11] Sun, S., Brandt, M. and Dargusch, M.S. (2009). Characteristics of cutting forces and chip formation in machining of titanium alloys, International Journal of Machine Tools and Manufacture, Vol. 49, pp. 561-568.

[12] Bayoumi, A.E. and Xie, J.Q. (1995). Some metallurgical aspects of chip formation in cutting Ti-6wt.%Al-4wt%V alloy, Materials Science and Engineering A, Vol. 190, pp. 173-180.

[13] Wan, Z.P., Zhu, Y.E., Liu, H.W. and Tang, Y. (2012). Microstructure evolution of adiabatic shear bands and mechanisms of saw-tooth chip formation in machining Ti6Al4V, Materials Science and Engineering A, Vol. 531, pp. 155-163.

[14] Sun, J. and Guo, Y.B. (2008). A new multi-view approach to characterize 3D chip morphology and properties in end milling titanium Ti-6Al-4V, International Journal of Machine Tools and Manufacture, Vol. 48, pp. 1486-1494.

[15] Boadu, M.K., Abankwa, E.O. and Anaba, L.A. (2018). Prediction of Chip Morphology for Aluminum Metal Matrix Composites in End Milling Machining, International Journal of Engineering Science and Technology (IJEST), Vol. 10, pp. 268-274

[16] Kouadri, S., Necib, K., Atlati, S., Haddag, B and Nouari, M. (2013). Quantification of the chip segmentation in metal machining: Application to machining the aeronautical aluminium alloy AA2024-T351 with cemented carbide tools WC-Co., Int. J. Mach. Tools Manuf., Vol 64, pp. 102-113.

[17] Komanduri, R., Schroeder, T.A., Bandhopadhyay, D.K. and Hazra, J. (1982). Titanium: A model material for analysis of the high-speed machining process advanced processing methods for titanium. D.F. Hasson, C.H. Hamilton (Eds.), the Metallurgical Society of ASME, pp. 241–256.

[18] Cook, N.H. (1953). Chip formation in machining titanium, Proceedings of the Symposium on Machine Grind. Titanium, Watertown Arsenal, MA, pp. 1–7

[19] Yameogo, D; Haddag, B; Makich, H; Nouari, M. (2017). Prediction of the cutting forces and chip morphology when machining the Ti6Al4V alloy using a microstructural coupled model, 16th CIRP Conference on Modelling of Machining Operations, Vol. 58, pp. 335 –340.

[20] Liu, C. R and Shi, J. (2006). On predicting chip morphology and phase transformation in hard machining, International Journal of Advanced Manufacturing Technology, Vol. 27, pp. 645-654.

[21] How Can Aerospace Benefit from 3D Printed Titanium Ti6Al4V? www.farinia.com. Retrieved June 7, 2019

[22] Properties of Titanium Alloy-Ti-6Al-4V. www.efunda.com. Retrieved June 7, 2019.